

Article

Stress and Damage Induced Gas Flow Pattern and Permeability Variation of Coal from Songzao Coalfield in Southwest China

Minghui Li ^{1,2,*}, Jie Cao ³ and Wenpu Li ^{1,2}

¹ State Key Laboratory of Coal Mine Disaster Dynamics and Control, Chongqing University, Chongqing 400030, China; wenpu617617@163.com

² College of Resource and Environmental Sciences, Chongqing University, Chongqing 400030, China

³ China Coal Technology Engineering Group Chongqing Research Institute, Chongqing 400030, China; cqcaoj@126.com

* Correspondence: cqumhli@vip.163.com; Tel.: +86-159-0238-8870

Academic Editor: Enrico Sciubba

Received: 18 March 2016; Accepted: 3 May 2016; Published: 7 May 2016

Abstract: The permeability of coal is a critical parameter in estimating the performance of coal reservoirs. Darcy's law describes the flow pattern that the permeability has a linear relationship with the flow velocity. However, the stress induced deformation and damage can significantly influence the gas flow pattern and permeability of coal. Coals from Songzao coalfield in Chongqing, southwest China were collected for the study. The gas flow velocities under different injection gas pressures and effective stresses in the intact coal and damaged coal were tested using helium, incorporating the role of gas flow pattern on the permeability of coal. The relationships between the flow velocity and square of gas pressure gradient were discussed, which can help us to investigate the transformation conditions of gas linear flow and gas nonlinear flow in the coal. The results showed that the gas flow in the intact coal existed pseudo-initial flow rate under low effective stress. The low-velocity non-Darcy gas flow gradually occurred and the start-up pressure gradient increased in the coal as the effective stress increased. The gas flow rate in the damaged coal increased nonlinearly as the square of pressure gradient increased under low effective stress. The instability of gas flow caused by high ratio of injection gas pressure over effective stress in the damaged coal contributed to the increase of the gas flow rate. As the effective stress increased, the increase of gas flow rate in coal turned to be linear. The mechanisms of the phenomena were explored according to the experimental results. The permeability of coal was corrected based on the relationships between the flow velocity and square of gas pressure gradient, which showed advantages in accurately estimating the performance of coal reservoirs.

Keywords: effective stress; coal permeability; gas flow pattern; Darcy's law; coal mine methane

1. Introduction

The permeability and gas flow pattern of coal play significant roles in controlling methane production of coal reservoirs [1,2]. The permeability of coal is greatly affected by the degree of damage, which is related to the deformation of coal [3,4]. The gas flow patterns of coal determine the calculation methods of the permeability. The gas flow in original multi-pore media reservoirs is usually regarded as a steady and linear process and can be described by Darcy's law. However, the gas flow pattern is also effected by stress induced deformation and damage. The low-velocity non-Darcy gas flow occurs in tight multi-pore media reservoirs. Meanwhile, the gas flow in damaged multi-pore media reservoirs may be unstable.

The permeability evolution of coal and rock has been investigated in recent years. The effects of pore pressure, effective stress, fluid saturation and adsorption/sorption properties on the permeability of coal have been recognized and documented [5–8]. The relative permeability of gas and water in different rank coals selected from south Qinshui Basin has been investigated under various gas/water saturations [9]. Moreover, the relations among matrix shrinkage, gas slippage, and permeability were explored [10–13]. Zhang *et al.* conducted the experiments to investigate relations among the flow rate, permeability and fracture aperture in fractured media [14]. Empirical relations based on laboratory results have been proposed to describe the relations among stress, permeability and porosity of sedimentary rock [15]. Cai *et al.* explored the contribution of stress and damage on the evolution of permeability through X-ray CT images and acoustic emission profiling together with concurrent measurements of the P-wave velocity [16]. For simultaneous exploitation of coal and coal mining methane (CMM), mining-enhanced permeability of coal has been tested in recent studies [17,18]. The deformation, strength and permeability evolution were studied through the conventional triaxial compression of initially intact coal [19]. Xie *et al.* proposed a unique model to describe the spatial and temporal distribution of coal permeability within the effective influence zone [20].

Klinkenberg proposed that the permeability constant as determined with gases is dependent upon the property of the gas, and is a linear function of the reciprocal mean pressure [21]. This effect can be explained by taking into account the phenomena of slip, which are related closely to the mean free paths of the gas molecules. The start-up pressure gradient exists under low permeability conditions was later reported and investigated [22,23]. Forchheimer proposed Darcy's law is inaccurate to describe high-velocity gas flow in porous media and added a second order of the velocity term to represent the microscopic inertial effect [24], which is proportional to the square of the flow velocity, to the pressure drop predicted by Darcy's law in order to account for the deviation,

$$-dP/dx = \mu v/K + \beta \rho v^2 \quad (1)$$

where P is pore pressure, μ is gas kinematic viscosity, v is gas flow velocity, β is non-Darcy coefficient and ρ is fluid density.

Non-Darcy flow in porous media was similar to turbulent flow in a conduit, the Reynolds number for identifying turbulent flow in conduits was adapted to describe non-Darcy flow in porous media [25]. Nashawi presented a semi-analytical equation that incorporates the effects of non-Darcy flow in the fracture and investigated the various parameters that influence the flow behavior of real gas in the fracture nearby the wellbore [26]. Zeng and Zhao proposed a rigorous semi-analytical model to study the production rate behavior of wells in gas reservoirs with Forchheimer's non-Darcy flow under constant or varying bottom-hole pressure conditions [27]. Mahdiyari *et al.* developed a number of simulators to study and compare the productivity of a hydraulically fractured well at both steady and pseudo steady states conditions [28]. The increase of flow rate in the samples tested by Jasinge *et al.* was non-linear at low confining pressures [29]. The investigation of fluid flow in post-peak porous media showed that the flow was deviated from Darcy's flow and the inertial coefficient β could be negative [30].

As shown in Figure 1, the stability of surrounding coal and rock near wellbores or boreholes depends on the relations between redistributed stress and strength of surrounding coal and rock. As redistributed stress reaches the strength, surrounding coal and rock will be damaged. The coal and rock is released and the permeability increases in this zone. The stress near wellbores or boreholes transfer to deep-seated rock and concentrated stress zone is generated in a certain range. The coal and rock are compressed and the permeability decreases in this zone. The degrees of coal damage in different zones are distinct as shown in Figure 2. The permeability and gas flow pattern of coal in different zones may be distinct as well. This study investigated the stress and damage-induced gas flow pattern and permeability variation of coal.

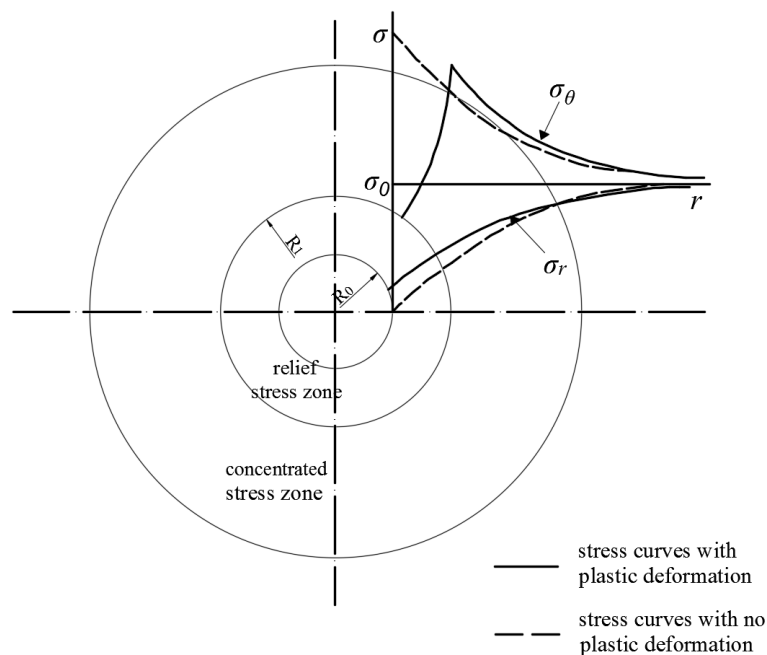


Figure 1. Stress redistribution and zones near wellbores or boreholes.

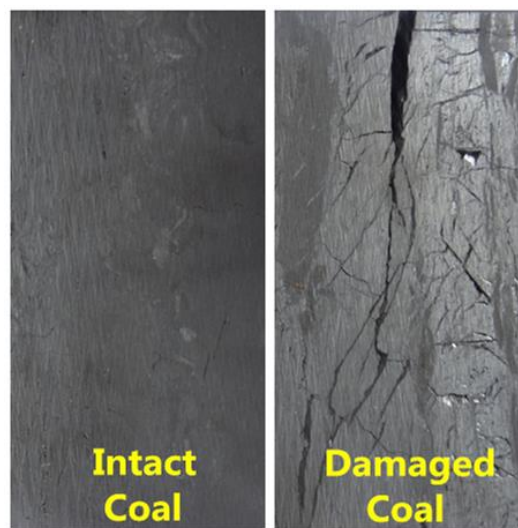


Figure 2. Coals with different degrees of damage.

2. Experimental Results and Analysis

2.1. Characteristics of Gas Flow Rate and Pattern Change in the Intact Coal and Damaged Coal

Figure 3 presents the relations between gas flow rate and effective stress of the intact coal and damaged coal (injection pressure = 1, 2, 3 and 4 MPa). It is noted that the gas flow rates increased with increasing injection pressure. This is consistent with the earlier studies [31]. Figure 3 reveals that the gas flow rates in both the intact coal and damaged coal decreased with increasing effective stress. This was because the coal was compressed as the effective stress increased, which narrowed the gas flow channels in the coal. The gas flow rates in the damaged coal under different effective stresses and injection pressures was range from 0.086 to 13.542 L/min and that in the intact coal was range from immeasurable to 0.0671 L/min. The gas flow rate in the damaged coal was higher than that in the intact coal by two to three orders of magnitude.

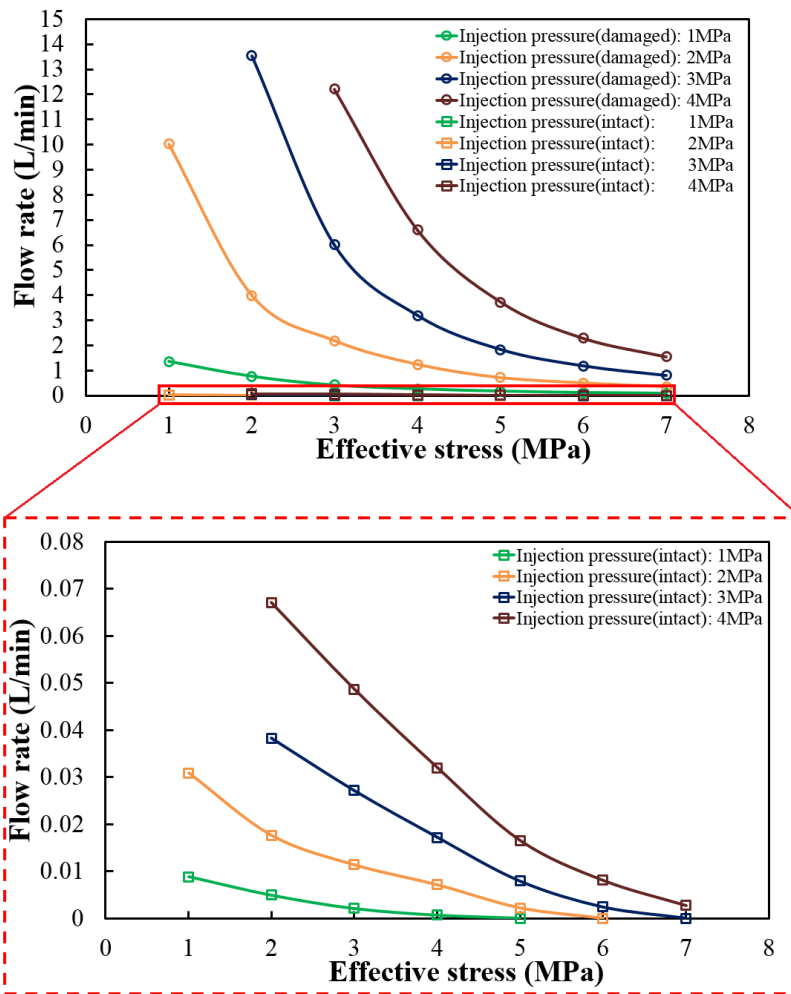


Figure 3. The relations between gas flow rate and effective stress.

Empirical relations between the gas flow rates and effective stresses of both the intact coal and damaged coal have been proposed. The logarithmic relation was found to be available for providing the highest coefficients of determination R^2 of fitting curves. The fitting equation is shown as below,

$$q = a \ln(\sigma_e) + b \tag{2}$$

where q is the gas permeation rate (m^3/s), σ_e is the effective stress (MPa), a and b are the fitting parameters related to material properties. The “ a ” decreased and the “ b ” increased with increasing injection pressure according to the experimental results. The fitting parameters and coefficients of determination under different injection pressures are shown in Table 1.

Table 1. Fitting parameters and coefficients of determination.

Injection Pressure (Intact Coal)	a	b	R^2	Injection Pressure (Damaged Coal)	a	b	R^2
1 MPa	−0.006	0.009	0.993	1 MPa	−0.664	1.264	0.966
2 MPa	−0.017	0.030	0.997	2 MPa	−4.806	8.5659	0.904
3 MPa	−0.032	0.061	0.993	3 MPa	−9.871	18.453	0.900
4 MPa	−0.054	0.105	0.994	4 MPa	−12.580	24.977	0.944

Figure 4 presents the relations between gas flow rate and square of pressure gradient in the intact coal (Results of the other specimens are shown in Figures S1 and S2). The gas flow rate in the intact coal increased linearly as the square of pressure gradient increased under low effective stress (effective stress = 1 and 2 MPa). However, the curves of gas flow rate *vs.* square of pressure gradient under low effective stress did not pass through the origin point. Pseudo-initial flow rates were observed in the experiments. Gas slippage effect, also known as Klinkenberg effect may account for this phenomenon. Pseudo-initial flow rate represents the level of slippage force. Based on the pseudo-initial flow rate, the relations between gas flow rate and square of pressure gradient in the intact coal under low effective stress should be described as follow,

$$A(P_1^2 - P_2^2)/2LP_2 = \mu(q - q_{pi})/K \quad (3)$$

where K is the permeability (m^2), L is the length of the coal specimens (m), A is the cross-sectional area of the coal specimens (m^2), P_1 is the gas pressure at the upper stream or inlet of specimens (Pa), and P_2 is the gas pressure at the downstream or outlet of the specimens (Pa), and q_{pi} is the pseudo-initial flow rate.

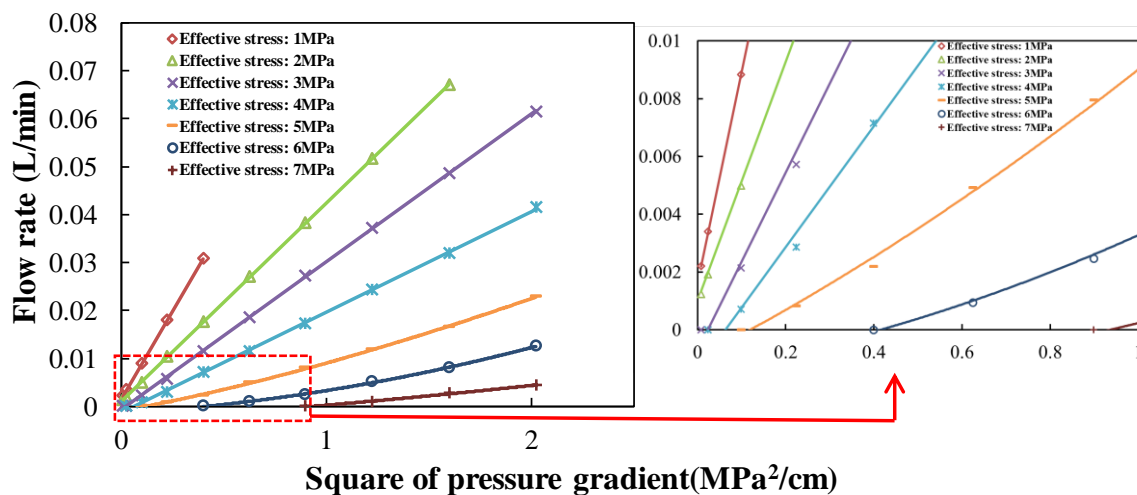


Figure 4. The relations between gas flow rate and square of pressure gradient in the intact coal.

As the effective stress increased, the start-up pressure gradients were observed. The critical point exists to divide the curve of gas flow rate *vs.* square of pressure gradient into two parts. The front part of the curve before the critical point is concave up and the other part of the curve after the critical point is approximately linear, which is regarded as low-velocity non-Darcy flow. The start-up pressure gradient increased as the effective stress increased, which indicated that the mobility of gas in the coal was weakened. The start-up pressure gradient represents the level of frictional resistance. The surface molecular force on the interface between solid phase and gas phase may account for this phenomenon. The force increased as the distance from fluid particle to the interface decreased with increasing effective stress. Gas can overcome the resistance to flow continuously as the pressure gradient increased. Based on the start-up pressure gradient, the relations between gas flow rate and square of pressure gradient in the intact coal should be described as follow,

$$A(P_1^2 - P_2^2 - J)/2LP_2 = \mu q/K \quad (4)$$

where J is the start-up pressure gradient.

Figure 5 presents the relations between gas flow rate and square of pressure gradient in the damaged coal. Figure 5 reveals that the gas flow rate in the damaged coal increased nonlinearly as the square of pressure gradient increased under low effective stress (effective stress = 1, 2 and 3 MPa).

The curves of gas flow rate *vs.* square of pressure gradient under low effective stress were concave up. Meanwhile, pseudo-initial flow rates were observed in the experiments. As the effective stress increased, the increase of gas flow rate in the coal turned to be linear and the curves turned to be straight. Based on the quadratic function relation and pseudo-initial flow rate, the relations between gas flow rate and square of pressure gradient in the damaged coal under low effective stress should be described as follow,

$$A(P_1^2 - P_2^2)/2LP_2 = \mu(q - q_{pi})/K + \alpha(q - q_{pi})^2 \quad (5)$$

where α is the coefficient of additional acceleration or resistance, and the second term to Darcy's equation, proportional to the velocity squared, is introduced to describe additional acceleration or resistance.

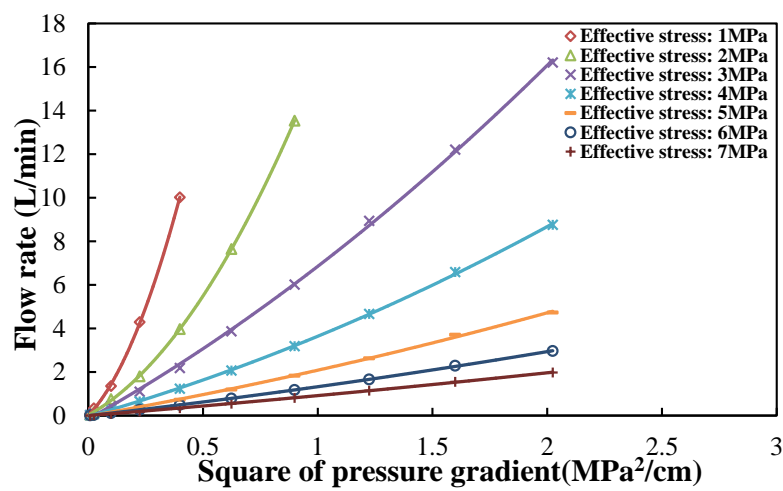


Figure 5. The relations between gas flow rate and square of pressure gradient in the damaged coal.

Equation (5) has a similar form with Forchheimer's equation. Forchheimer's equation is normally used to describe the high-velocity non-Darcy flow, where the inertial coefficient β was defined. A second term to Darcy's equation, proportional to the velocity squared, was introduced to describe inertial resistance. The inertial coefficient β is usually positive in high-velocity non-Darcy flow, which means that the flow rate is decreased by inertial resistance. However, the gas flow rate in the experiment of the damaged coal under low effective stress was increased. And the coefficient of additional acceleration or resistance α was negative in the damaged coal under low effective stress. Forchheimer's equation is derived based on the assumption of rigid skeleton in coal, which is able to describe the pressure drop induced by inertial effect but limited to considerate the instability of gas flow caused by high ratio of injection gas pressure over effective stress in the damaged coal. In the damaged coal, the original skeleton was damaged and recombined. The increasing injection gas pressure under low effective stress promoted the damage and recombination of the coal, which led to the erosion of coal particles. Therefore, the gas flow in the damaged coal under low effective stress was an unsteady process. The above phenomena would enhance the permeability of the damaged coal. Thus, the flow rate of the damaged coal under low effective stress increased with increasing injection pressure and the coefficient of additional acceleration or resistance α was negative.

2.2. Characteristics of Permeability Change in the Intact Coal and Damaged Coal

Figure 6 presents the apparent permeability and corrected absolute permeability in the intact coal under different injection pressures and effective stresses. Figure 6 reveals that the apparent permeability in the intact coal calculated by Darcy's law decreased (effective stress = 1 and 2 MPa) or increased (effective stress = 3, 4, 5, 6 and 7 MPa) with increasing injection pressure under the same effective stresses, whereas the absolute permeability corrected by Equations (3) and (4) stayed constant

with increasing injection pressure. The permeability in the intact coal should be constant under a same effective stress as the skeleton of coal and flow channels for gas remain unchanged. The deviation of the apparent permeability calculated by Darcy’s law is the result of ignoring the Klinkenberg effect and frictional resistance. Figure 6a presents the difference between the apparent permeability and corrected absolute permeability caused by Klinkenberg effect. Figure 6a reveals that the apparent permeability in the intact coal calculated by Darcy’s law decreased with increasing injection pressure. The apparent permeability was higher than the corrected absolute permeability. The apparent permeability was enhanced from the absolute permeability by Klinkenberg effect. Figure 6b presents the difference between the apparent permeability and corrected absolute permeability caused by frictional resistance. Figure 6b reveals that the apparent permeability in the intact coal calculated by Darcy’s law increased with increasing injection pressure. The apparent permeability was lower than the corrected absolute permeability. The apparent permeability was reduced from the absolute permeability by frictional resistance. The corrected absolute permeability of the intact coal was more accurate, and showed advantages in estimating the performance of coal reservoirs.

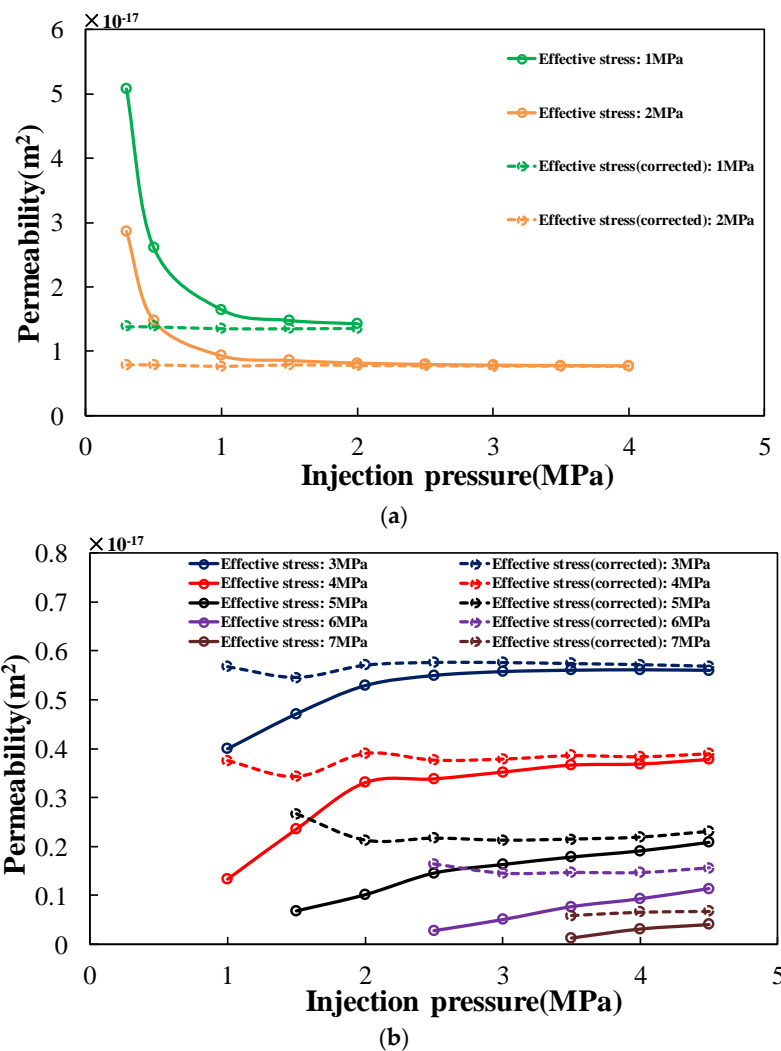


Figure 6. The apparent permeability and corrected absolute permeability in the intact coal under different injection pressures and effective stresses: (a) the difference between the apparent permeability and corrected permeability caused by Klinkenberg effect; and (b) the difference between the apparent permeability and corrected permeability caused by frictional resistance.

To obtain the characteristics of permeability in the damaged coal, Equation (5) can be transformed into:

$$A(P_1^2 - P_2^2)/2LP_2 = [\mu/K + \alpha(q - q_{pi})](q - q_{pi}) \tag{6}$$

where $\alpha(q - q_{pi})/\mu$ represents the instability of gas flow induced permeability increase. Equation (6) can be transformed into:

$$A(P_1^2 - P_2^2)/2LP_2 = \mu(q - q_{pi}) / \{K\mu / [\mu + K\alpha(q - q_{pi})]\} \tag{7}$$

where $K_{real} = K\mu / [\mu + K\alpha(q - q_{pi})]$ is defined to be the permeability in the damaged coal under low effective stress, which increases with increasing q as the result of instability of gas flow induced by high ratio of injection gas pressure over effective stress. Therefore, Equation (7) can be transformed into:

$$A(P_1^2 - P_2^2)/2LP_2 = \mu(q - q_{pi}) / K_{real} \tag{8}$$

Figure 7 presents the permeability in the damaged coal under different injection pressures and effective stresses. Figure 7 reveals that the permeability in the damaged coal under low effective stress increased with increasing injection pressure. This is due to the original skeleton in the coal was damaged and recombined, and the increasing injection gas pressure under low effective stress promoted the damage and recombination of coal, which led to the erosion of coal particles. As the effective stress increased, the permeability in the damaged coal turned to be constant with increasing injection pressure.

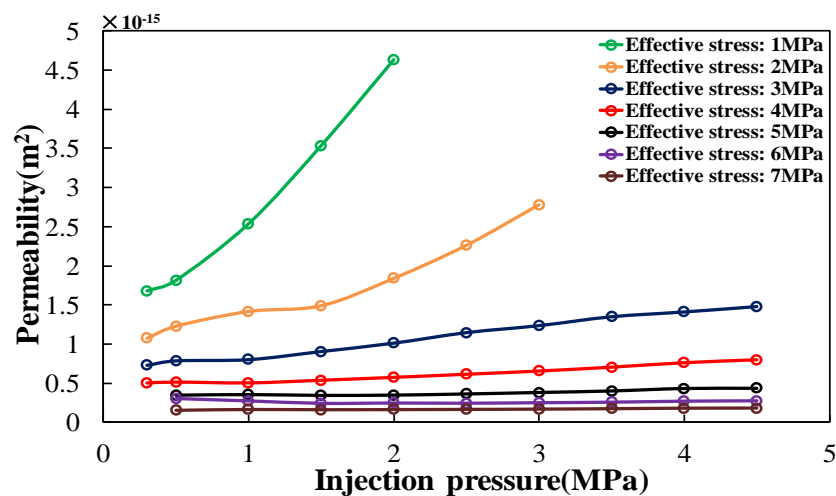


Figure 7. The permeability in the damaged coal under different injection pressures and effective stresses.

Figure 8 presents the permeability against confining stress at the same injection pressure. Figure 8 reveals that the permeability in both the intact coal and damaged coal decreased with increasing confining stress. This was because the coal was compressed as the confining stress increased, which narrowed the gas flow channels in the coal. The permeability in the damaged coal was higher than that in the intact coal by two to three orders of magnitude. This is caused by the differences between the microscopic structures of the intact coal and damaged coal. Figure 9 presents the microscopic structures of the intact coal and damaged coal. No obvious fractures were observed in the intact coal. However, connecting and obvious fractures were observed in the damaged coal. Fractures are the main channels for gas flow, thus enhance the permeability in coal.

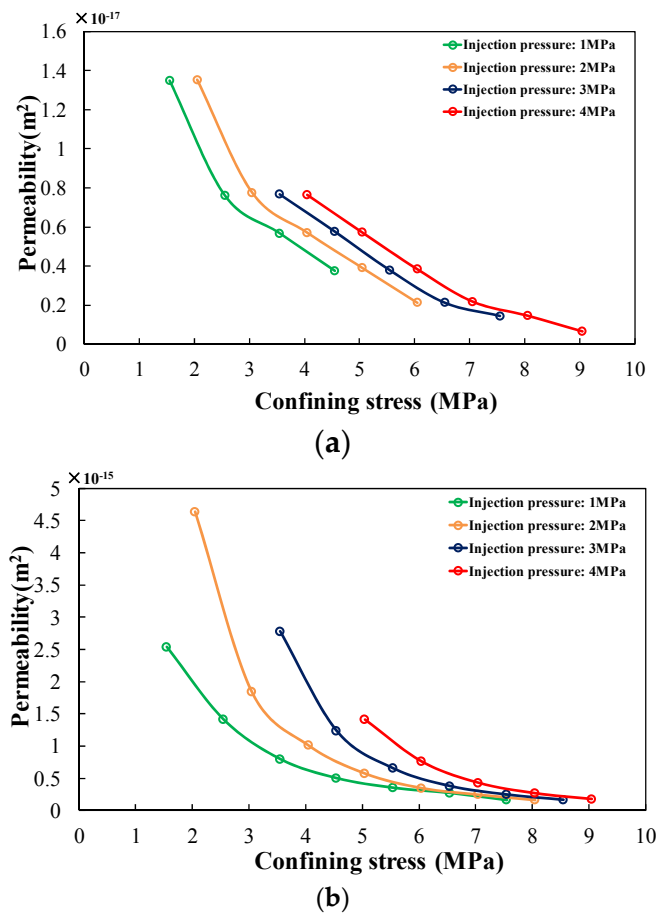


Figure 8. The permeability against confining stress at the same injection pressure: (a) permeability against confining stress in intact coal; and (b) permeability against confining stress in damaged coal.

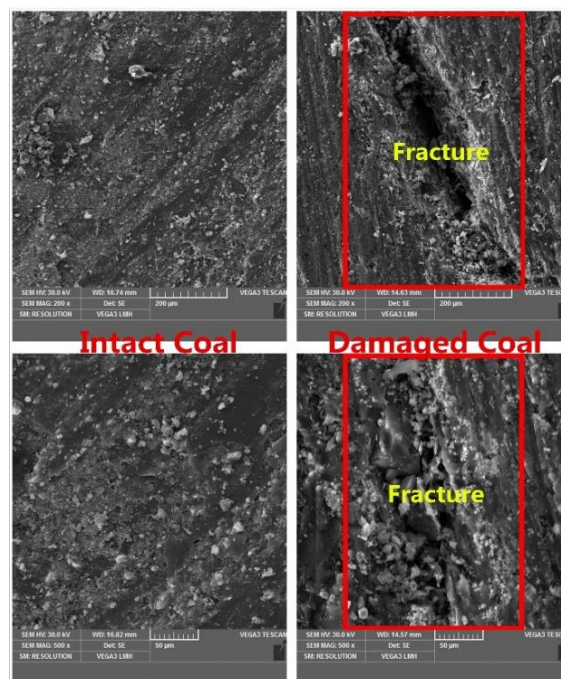


Figure 9. Microscopic structures of the intact coal and damaged coal.

3. Experiment Setup for Tests

3.1. Experiment Apparatus

The experiments were conducted by using the newly self-made “Thermo-hydro-mechanical (THM) coupled with triaxial servo-controlled seepage apparatus for coal and rock” (THM-2 style). The newly-developed apparatus is applicable to investigate the combined effect of stress, strain, temperature and gas flow on the mechanical behavior and permeability evolution of coal and rock. This apparatus has following technical specifications: the maximum axial force of 1000 kN, the maximum confining pressure of 60 MPa, the maximum gas pressure of 20 MPa, the maximum axial displacement of 60 mm, and the maximum radial deformation of 12 mm. An oil tank is used to adjust the experiment temperature from room temperature to 110 °C. The accuracy of this measurement system is $\pm 1\%$ for stress, $\pm 1\%$ for deformation, and ± 0.1 °C for temperature control. Figure 10 shows the apparatus.

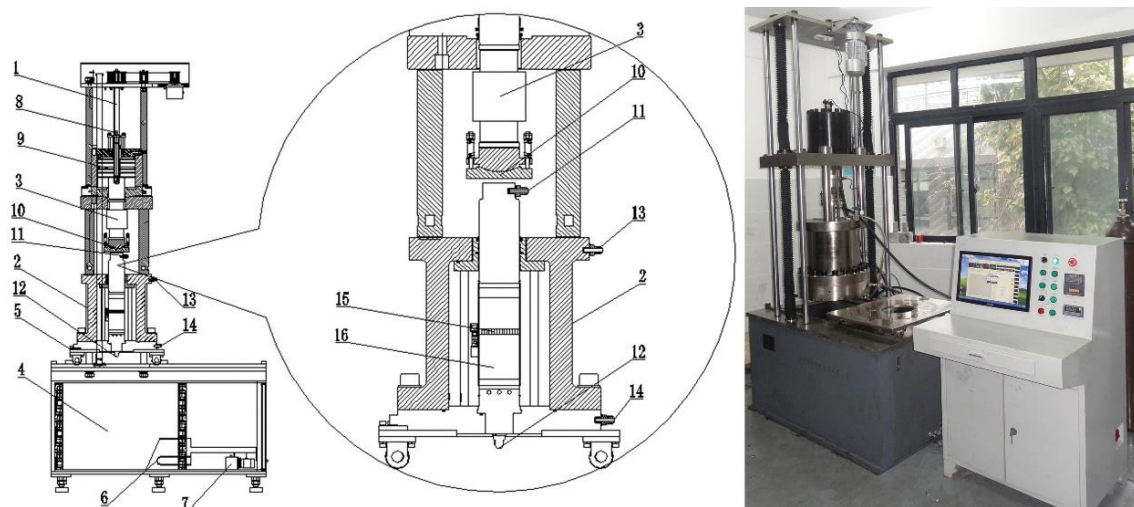


Figure 10. Thermo-Hydro-Mechanical (THM) coupling with triaxial servo-controlled seepage apparatus for coal and rock: 1—Lifter; 2—Pressure vessel; 3—Sensor of axial stress; 4—Oil tank; 5—Movable work platform; 6—Heater tubes; 7—Oil inlet valve; 8—Sensor of axial displacement; 9—Hydraulic cylinder of axial stress; 10—Force plate; 11—Gas inlet valve; 12—Gas outlet valve; 13—Air drain valve; 14—Hydraulic oil inlet and drain valve; 15—Circumferential extensometers; 16—Specimens.

The following are designed to improve the accuracy of loading and measurement. The servo hydraulic pressure controller performs continuous loading/unloading paths. A high-permeable pad with multi-holes is designed to let gas pass through the specimen uniformly. The constant temperature oil heating system is designed to keep the temperature constant. The stress, strain, temperature, and gas flow rate are automatically measured by high accuracy sensors. The loading system is continuously controlled by a computer. This apparatus has system rigidity greater than 10 GN/m and is thus suitable for displacement control.

3.2. General Geology of the Sampling Area

The specimens were gathered from coal seam K₂b of Songzao coalfield in Chongqing, southwest China. The geological map of Songzao coalfield highlighting the sampling area in the field is shown in Figure 11. Table 2 lists the geological profiles of the coal seam. The elevation in the area ranges from 360 to 1300 masl. The oldest outcropping strata in the area is the Middle Silurian Hanjiadian formation, and the newest outcropping strata in the area is the Upper Triassic Xujiahe formation. The coal-bearing

strata is the Permian Longtan formation. The coal-bearing strata shows marine-continental transitional facies. The overburden depth ranges between 500 and 540 m with a 460–500 m thick alluvium layer at the top. It has a dip angle ranging from 35° to 37° and an average thickness of 0.75 m, ranging from 0.22 m to 1.20 m. The coal seam K₂b is a gas infiltrated layer, with a gas content of 10.14 m³/t. The temperature in the coal seam K₂b is in the range of 28.5 °C to 29.3 °C. The average vitrinite content of the coal is 68.4%, inertinite content is 18.7%, clay mineral content is 8.4%, oxide content is 2.0%, carbonate content is 0.4%, and sulfide content is 2.1%.

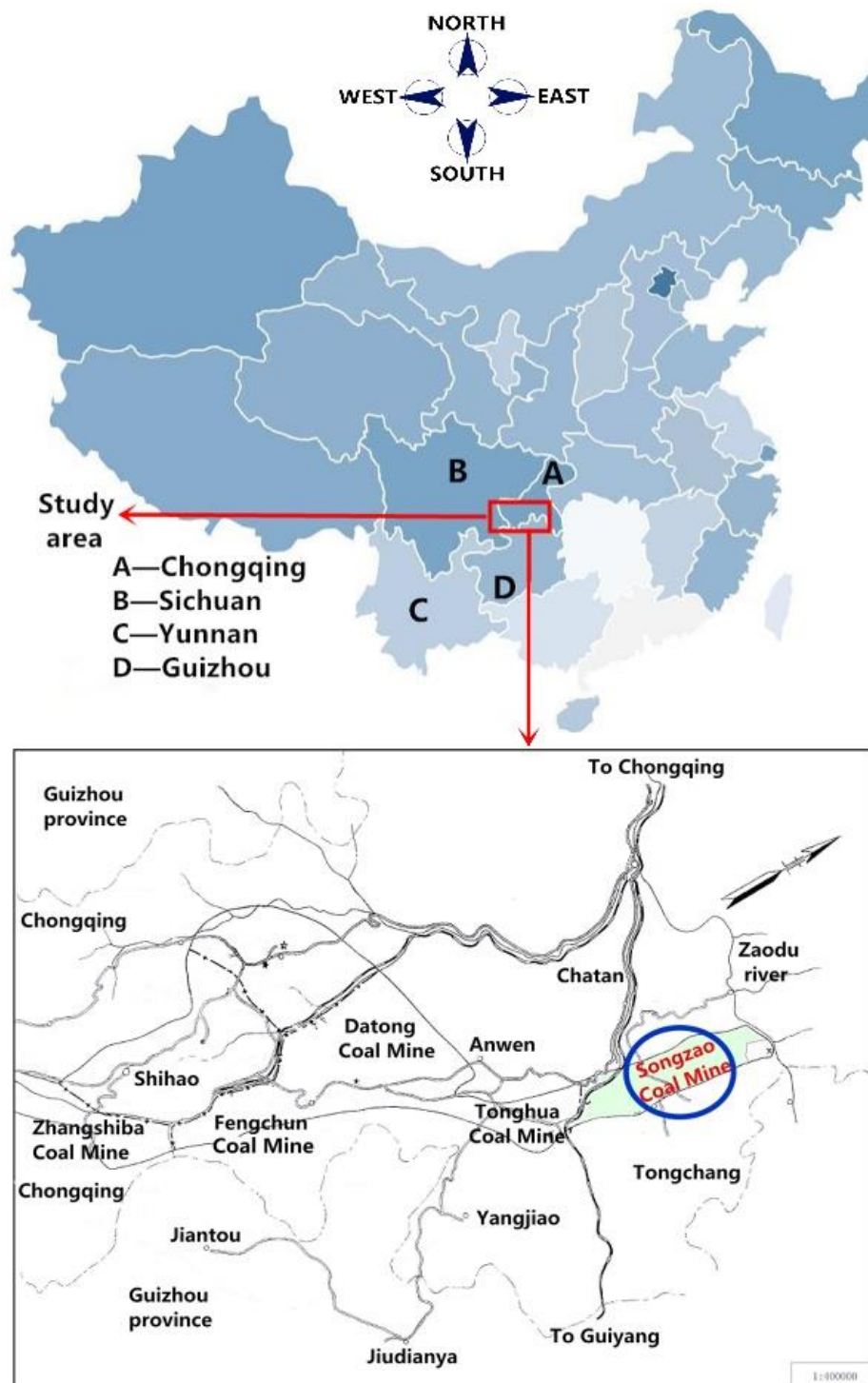


Figure 11. Geological map of Songzao coalfield highlighting the sampling area in the field.

Table 2. Simplified geological profiles of coal seam K₂b.

Layer Number	Lithology	Thickness (m)
1	Alluvium	460
2	Sandstone	5.45
3	Sandy mudstone	2.65
4	Coal seam	1.83
5	Sandy mudstone	7.43
6	Limestone	1.25
7	Sandstone	3.96
8	Limestone	1.01
9	Sandy mudstone	3.18
10	Argillaceous limestone	4.90
11	Coal seam	0.75
12	Sandy mudstone	3.72
13	Coal seam	0.24
14	Sandy mudstone	3.41
15	Siliceous limestone	1.56
16	Calcareous mudstone	1.19

3.3. Characterisation of Coal

Proximate, structure and geotechnical analyses were carried out for the characterization of coal specimen used for the experiment, and the summary of results is shown in Table 3.

Table 3. Main characteristic parameters of the coal.

BET Surface Area (m ² /g)	Langmuir Surface Area (m ² /g)	Total Pore Volume (cm ³ /g)	Average Pore Width (Å)	Mad (%)	Aad (%)	Vad (%)	Fcad (%)
0.2997	0.4744	0.0014	189.5302	1.17	13.16	21.03	64.64
UCS (MPa) 14.72	Density (kg/m ³) 1460	Young's Modulus (GPa) 4.77		Poisson's ratio 0.21			

Mad—moisture content on air dried basis; Aad—ash content on air dried basis; Vad—volatile content on air dried basis; Fcad—fixed carbon content on air dried basis. UCS—uniaxial compressive strength.

3.4. Specimen Preparation

Large intact coal blocks were collected and treated from the coal seam according to the “general requirements for sampling (China National Code of GB/T 23561.1-2009)”. The coal blocks were shaped into cylindrical specimens of Φ 50 mm \times 100 mm. The specimen determined to be without visible fractures and cracks, by means of photo observation and statistical classification, was chosen as the experimental specimen. Figure 12 shows the specimen.

**Figure 12.** The collected specimen.

3.5. Experiment Procedure and Data Treatment

According to Harpalani and Chen [32], and as also mentioned by Ranjith and Perera [33], the effective stress is a function of gas pressure as shown in the following equation,

$$\sigma_e = \sigma_c - \frac{P_i + P_0}{2} \quad (9)$$

where σ_c is the confining pressure (MPa), P_i is the gas injection pressure (MPa) and P_0 is the gas outlet pressure (atmospheric pressure for the experiment).

Based on the effective stress, the conditions used in the experiment were illustrated in Figure 13 and described as below.

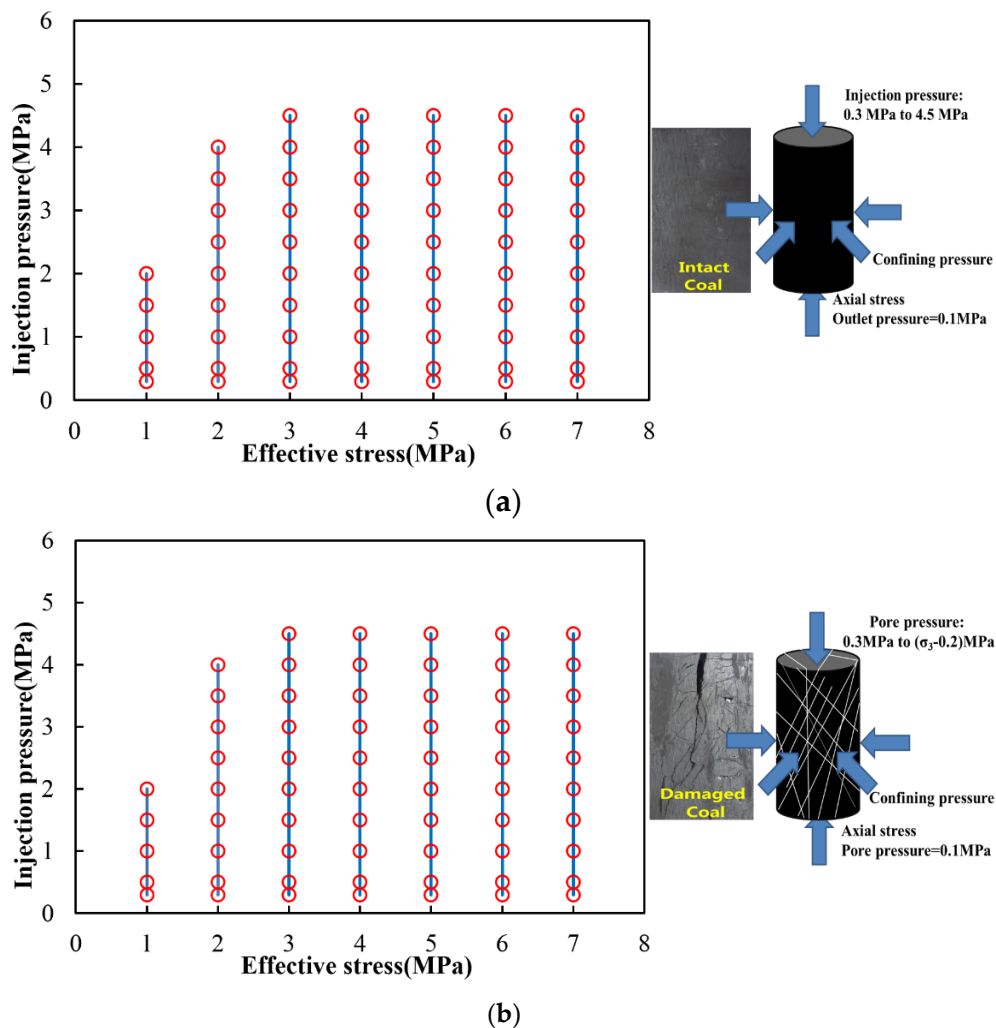


Figure 13. The experimental stress and injection pressure conditions: (a) Condition 1; and (b) Condition 2. Red circles are the measured points.

Condition 1: The isotropic *in-situ* stress states of $\sigma_e = 1, 2, 3, 4, 5, 6$ and 7 MPa were applied to the specimen, respectively. Then, the high-pressure helium tank was connected to the specimen to inject the inert gas helium into the specimen up to the specified injection pressure (from 0.3 to 4.5 MPa). The gas flow rate at each pressure point was measured.

Condition 2: The isotropic *in-situ* stress state of $\sigma_e = 7$ MPa (injection pressure = 4.5 MPa) was applied to the specimen that was used in the experiment of Condition 1. The deviatoric stress was then applied to the specimen with a speed of 0.1 mm/min till its post-peak stage. Then, the stress was

released. The isotropic *in-situ* stress states of $\sigma_e = 1, 2, 3, 4, 5, 6$ and 7 MPa were applied again to the specimen, respectively. The corresponding injection pressure was injected and the flow rate of gas at each pressure point was measured.

The experiments strictly followed the following test procedure. Silicon rubber was evenly coated on the coal specimen to prevent gas leakage from the coal. The specimen was installed between the top and bottom pressure shafts in the triaxial chamber after the silicone rubber was fully dry. A thermal shrunken pipe was then put on. This pipe was heated by a heater so that it closely contacted the specimen wall and both ends of the pressure shafts. The thermal shrunken pipe was then tightened by metal hoops at both ends of the pressure shafts. A circumferential extensometer and the remaining parts of the triaxial flow apparatus were then installed.

The gas permeation through the specimen was assumed to be isothermal, and helium was ideal gas. According to Darcy's law, the permeability of coal was calculated by [34],

$$K = \frac{2q\mu LP_2}{A(P_1^2 - P_2^2)} \quad (10)$$

4. Conclusions

Coals from Songzao coalfield in Chongqing, southwest China were tested using inert gas helium to obtain the gas flow velocities under different injection gas pressures and effective stresses in intact coal and damaged coal, incorporating the role of gas flow pattern on the permeability of coal. The relations between flow velocity and square of gas pressure gradient were discussed, which can help us investigate the transformation conditions of gas linear flow and gas nonlinear flow in the coal. The mechanisms of the phenomena are explored according to the experimental results. The permeability of coal was corrected based on the relations between flow velocity and square of gas pressure gradient, which showed advantages in accurately estimating the performance of coal reservoirs. Based on these results, the following understandings and conclusions can be drawn:

- (1) Both the gas flow rates in the intact coal and damaged coal increased with increasing injection pressure. The gas flow rate in the damaged coal was higher than that in the intact coal by two to three orders of magnitude. The logarithmic relation was found to be available for providing the highest coefficients of determination R^2 of fitting curves to describe the relations between the gas flow rates and effective stresses of both the intact coal and damaged coal.
- (2) Pseudo-initial flow rates were observed in the intact coal under low effective stress. Klinkenberg effect may account for this phenomenon. Pseudo-initial flow rate represents the level of slippage force. Based on the pseudo-initial flow rate, the equation to describe relations between gas flow rate and square of pressure gradient in the intact coal under low effective stress has been proposed. As the effective stress increased, the start-up pressure gradients were observed. The start-up pressure gradient increased as the effective stress increased, which indicated that the mobility of gas in the coal was weakened. The start-up pressure gradient represents the level of frictional resistance. Based on the start-up pressure gradient, the equation to describe the relations between gas flow rate and square of pressure gradient in the intact coal has been proposed.
- (3) The gas flow rate in the damaged coal increased nonlinearly as the square of pressure gradient increased under low effective stress. As the effective stress increased, the increase of gas flow rate in the coal turned to be linear. Based on the quadratic function relation and pseudo-initial flow rate, the equation to describe the relations between gas flow rate and square of pressure gradient in the damaged coal under low effective stress has been proposed. In the damaged coal, the original skeleton was damaged and recombined. The increasing injection gas pressure under low effective stress promoted the damage and recombination of coal, which led to the erosion of coal particles. The phenomena would enhance the permeability of coal. Therefore, the coefficient of additional acceleration or resistance α was negative.

- (4) The apparent permeability in the intact coal calculated by Darcy's law decreased or increased with increasing injection pressure under the same effective stresses. Whereas, the absolute permeability corrected by the analysis above stayed constant with increasing injection pressure. The deviation of the apparent permeability calculated by Darcy's law is the result of ignoring the Klinkenberg effect and frictional resistance. The corrected absolute permeability of the intact coal showed advantages in accurately estimating the performance of coal reservoirs.
- (5) The permeability in the damaged coal under low effective stress increased with increasing injection pressure. As the effective stress increased, the permeability in coal turned to be constant with increasing injection pressure. Compared with the intact coal, more connecting and obvious fractures are observed in the damaged coal. Thus, the permeability in the damaged coal was higher than that in the intact coal by two to three orders of magnitude.

Supplementary Materials: The following are available online at <http://www.mdpi.com/1996-1073/9/5/351/s1>.

Acknowledgments: This study was financially supported by National Natural Science Foundation of China (51434003, 51374256), Chongqing Graduate Student Research Innovation Project (CYB14008) and Chongqing Research Program of Application Foundation and Advanced Technology (CSTC2015JCYJA90009). Authors are grateful to Songzao Coal & Electricity Company, Limited and Songzao coal mine in Chongqing, China for their help and technical support in obtaining the coals.

Author Contributions: Minghui Li conceived and designed the experiments; Wenpu Li performed the experiments; Minghui Li and Jie Cao analyzed the data; and Minghui Li wrote the paper.

Conflicts of Interest: The authors declare no conflict of interest.

References

1. Liu, Q.; Cheng, Y.; Yuan, L.; Tong, B.; Kong, S.; Zhang, R. CMM capture engineering challenges and characteristics of *in-situ* stress distribution in deep level of Huainan coalfield. *J. Nat. Gas Sci. Eng.* **2015**, *20*, 328–336. [[CrossRef](#)]
2. Wang, H.; Cheng, Y.; Wang, W.; Xu, R. Research on comprehensive CBM extraction technology and its applications in China's coal mines. *J. Nat. Gas Sci. Eng.* **2014**, *20*, 200–207. [[CrossRef](#)]
3. Yang, W.; Lin, B.; Qu, Y.; Zhao, S.; Zhai, C.; Jia, L.; Zhao, W. Mechanism of strata deformation under protective seam and its application for relieved methane control. *Int. J. Coal Geol.* **2011**, *85*, 300–306. [[CrossRef](#)]
4. Liu, T.; Lin, B.; Zou, Q.; Zhu, C.; Guo, C.; Li, J. Investigation on mechanical properties and damage evolution of coal after hydraulic slotting. *J. Nat. Gas Sci. Eng.* **2015**, *24*, 489–499. [[CrossRef](#)]
5. Vishal, V.; Ranjith, P.G.; Pradhan, S.P.; Singh, T.N. Permeability of sub-critical carbon dioxide in naturally fractured Indian bituminous coal at a range of down-hole stress conditions. *Eng. Geol.* **2013**, *167*, 148–156. [[CrossRef](#)]
6. Vishal, V.; Ranjith, P.G.; Singh, T.N. An experimental investigation on behaviour of coal under fluid saturation, using acoustic emission. *J. Nat. Gas Sci. Eng.* **2015**, *22*, 428–436. [[CrossRef](#)]
7. Vishal, V.; Singh, T.N.; Ranjith, P.G. Influence of sorption time in CO₂-ECBM process in Indian coals using coupled numerical simulation. *Fuel* **2015**, *139*, 51–58. [[CrossRef](#)]
8. Ranathunga, A.S.; Perera, M.S.A.; Ranjith, P.G.; Ju, Y.; Vishal, V.; De Silva, P.N.K. A macro-scale experimental study of sub—and super-critical CO₂ flow behaviour in Victorian brown coal. *Fuel* **2015**, *158*, 864–873. [[CrossRef](#)]
9. Shen, J.; Qin, Y.; Wang, G.; Fu, X.; Wei, C.; Lei, B. Relative permeabilities of gas and water for different rank coals. *Int. J. Coal Geol.* **2011**, *86*, 166–275. [[CrossRef](#)]
10. Pan, Z.J.; Connell, L.D.; Camilleri, M. Laboratory characterisation of coal reservoir permeability for primary and enhanced coalbed methane recovery. *Int. J. Coal Geol.* **2010**, *82*, 252–261. [[CrossRef](#)]
11. Li, J.Q.; Liu, D.M.; Yao, Y.B.; Cai, Y.D.; Chen, Y. Evaluation and modeling of gas permeability changes in anthracite coals. *Fuel* **2013**, *111*, 606–612. [[CrossRef](#)]
12. Chareonsuppanimit, P.; Mohammad, S.A.; Robinson, R.L., Jr.; Gasem, K.A.M. Modeling gas-adsorption-induced swelling and permeability changes in coals. *Int. J. Coal Geol.* **2014**, *121*, 98–109. [[CrossRef](#)]

13. Vishal, V.; Singh, T.N. A laboratory investigation of permeability of coal to supercritical CO₂. *Geotech. Geol. Eng.* **2015**, *33*, 1009–1016. [[CrossRef](#)]
14. Zhang, J.; Standifird, W.B.; Roegiers, J.C.; Zhang, Y. Stress-dependent fluid flow and permeability in fractured media: From lab experiments to engineering applications. *Rock Mech. Rock Eng.* **2007**, *40*, 3–21. [[CrossRef](#)]
15. Zheng, J.; Zheng, L.; Liu, H.; Ju, Y. Relationships between permeability, porosity and effective stress for low-permeability sedimentary rock. *Int. J. Rock Mech. Min. Sci.* **2015**, *78*, 304–318. [[CrossRef](#)]
16. Cai, Y.D.; Liu, D.M.; Jonathan, P.M.; Pan, Z.J.; Elsworth, D.; Yao, Y.B.; Li, J.Q.; Guo, X.Q. Permeability evolution in fractured coal-combining triaxial confinement with X-ray computed tomography, acoustic emission and ultrasonic techniques. *Int. J. Coal Geol.* **2014**, *122*, 91–104. [[CrossRef](#)]
17. Xie, H.; Xie, J.; Gao, M.; Zhang, R.; Zhou, H.; Gao, F.; Zhang, Z. Theoretical and experimental validation of mining-enhanced permeability for simultaneous exploitation of coal and gas. *Environ. Earth Sci.* **2015**, *73*, 5951–5962. [[CrossRef](#)]
18. Yin, G.; Li, M.; Wang, J.G.; Xu, J.; Li, W. Mechanical behavior and permeability evolution of gas infiltrated coals during protective layer mining. *Int. J. Rock Mech. Min. Sci.* **2015**, *80*, 292–301. [[CrossRef](#)]
19. Wang, S.G.; Elsworth, D.; Liu, J.S. Permeability evolution during progressive deformation of intact coal and implications for instability in underground coal seams. *Int. J. Rock Mech. Min. Sci.* **2013**, *58*, 34–45. [[CrossRef](#)]
20. Xie, J.; Gao, M.; Yu, B.; Zhang, R.; Jin, W. Coal permeability model on the effect of gas extraction within effective influence zone. *Geomech. Geophys. Geo-Energy Geo-Resour.* **2015**, *1*, 15–27. [[CrossRef](#)]
21. Klinkenberg, L.J. The permeability of porous media to liquids and gases. *Drill. Prod. Pract.* **1941**, 200–213.
22. Swartzendruber, D. Non-Darcy flow behavior in liquid-saturated porous media. *J. Geophys. Res.* **1962**, *67*, 5205–5213. [[CrossRef](#)]
23. Miller, R.J.; Low, P.F. Threshold gradient of water in clay systems. *Soil Sci. Soc. Am. J.* **1963**, *27*, 605–609. [[CrossRef](#)]
24. Forchheimer, P. Wasserbewegung Durch Boden. *Z. Ver. Deutsch. Ing.* **1901**, *45*, 1782–1788.
25. Hassanizadeh, S.M.; Gray, W.G. High velocity flow in porous media. *Trans. Porous Media* **1987**, *2*, 521–531. [[CrossRef](#)]
26. Nashawi, I.S. Constant-pressure well test analysis of finite-conductivity hydraulically fractured gas wells influenced by non-Darcy flow effects. *J. Pet. Sci. Eng.* **2006**, *53*, 225–238. [[CrossRef](#)]
27. Zeng, F.; Zhao, G. Gas well production analysis with non-Darcy flow and real-gas PVT behavior. *J. Pet. Sci. Eng.* **2007**, *59*, 169–182. [[CrossRef](#)]
28. Mahdiyari, H.; Jamiolahmady, M.; Sohrabi, M. Improved Darcy and non-Darcy flow formulations around hydraulically fractured wells. *J. Pet. Sci. Eng.* **2011**, *78*, 149–159. [[CrossRef](#)]
29. Jasinge, D.; Ranjith, P.G.; Choi, S.K. Effects of effective stress changes on permeability of Latrobe Valley brown coal. *Fuel* **2011**, *90*, 1292–1300. [[CrossRef](#)]
30. Miao, X.; Chen, Z.; Mao, X. The bifurcation of non-Darcy flow in post-failure rock. *Acta Mech. Sin.* **2003**, *35*, 660–667.
31. Vishal, V.; Ranjith, P.G.; Singh, T.N. CO₂ permeability of Indian bituminous coals: Implications for carbon sequestration. *Int. J. Coal Geol.* **2013**, *105*, 36–47. [[CrossRef](#)]
32. Harpalani, S.; Chen, G. Influence of gas production induced volumetric strain on permeability of coal. *Geotech. Geol. Eng.* **1997**, *15*, 303–325. [[CrossRef](#)]
33. Ranjith, P.G.; Perera, M.S.A. A new triaxial apparatus to study the mechanical and fluid flow aspects of carbon dioxide sequestration in geological formations. *Fuel* **2011**, *90*, 2751–2759. [[CrossRef](#)]
34. Hildenbrand, A.; Schlömer, S.; Krooss, B.M. Gas breakthrough experiments on fine-grained sedimentary rocks. *Geofluids* **2002**, *2*, 3–23. [[CrossRef](#)]

